Original

Schroeder, J.L.; Thomson, W.; Howard, B.; Schell, N.; Naeslund, L.-A.; Rogstroem, L.; Johansson-Joesaar, M.P.; Ghafoor, N.; Oden, M.; Nothnagel, E.; Shepard, A.; Greer, J.; Birch, J.:

Industry-relevant magnetron sputtering and cathodic arc ultra-high vacuum deposition system for in situ x-ray diffraction studies of thin film growth using high energy synchrotron radiation

In: Review of Scientific Instruments (2015) AIP

DOI: 10.1063/1.4930243

Industry-relevant magnetron sputtering and cathodic arc ultra-high vacuum deposition system for *in situ* x-ray diffraction studies of thin film growth using high energy synchrotron radiation

J. L. Schroeder,[1,a)] W. Thomson,[2] B. Howard,[2] N. Schell,[3] L.-Å. Näslund,[1] L. Rogström,[1] M. P. Johansson-Jõesaar,[4] N. Ghafoor,[1] M. Odén,[1] E. Nothnagel,[2] A. Shepard,[2] J. Greer,[2] and J. Birch[1]

[1]*Department of Physics, Chemistry, and Biology (IFM), Linköping University, SE-581 83 Linköping, Sweden*
[2]*PVD Products Inc., 35 Upton Dr., Suite 200, Wilmington, Massachusetts 01887, USA*
[3]*Helmholtz-Zentrum Geesthacht, Centre for Materials and Coastal Research, Institute for Materials Research, Max-Planck-Straße 1, 21502 Geesthacht, Germany*
[4]*Seco Tools AB, Björnbacksvägen 2, SE-737 82 Fagersta, Sweden*

(Received 16 May 2015; accepted 25 August 2015; published online 22 September 2015)

We present an industry-relevant, large-scale, ultra-high vacuum (UHV) magnetron sputtering and cathodic arc deposition system purposefully designed for time-resolved *in situ* thin film deposition/annealing studies using high-energy (>50 keV), high photon flux (>10^{12} ph/s) synchrotron radiation. The high photon flux, combined with a fast-acquisition-time (<1 s) two-dimensional (2D) detector, permits time-resolved *in situ* structural analysis of thin film formation processes. The high-energy synchrotron-radiation based x-rays result in small scattering angles (<11°), allowing large areas of reciprocal space to be imaged with a 2D detector. The system has been designed for use on the 1-tonne, ultra-high load, high-resolution hexapod at the P07 High Energy Materials Science beamline at PETRA III at the Deutsches Elektronen-Synchrotron in Hamburg, Germany. The deposition system includes standard features of a typical UHV deposition system plus a range of special features suited for synchrotron radiation studies and industry-relevant processes. We openly encourage the materials research community to contact us for collaborative opportunities using this unique and versatile scientific instrument. © *2015 AIP Publishing LLC.* [http://dx.doi.org/10.1063/1.4930243]

I. INTRODUCTION

Time-resolved *in situ* studies of thin film formation processes through the use of high-energy (>50 keV) synchrotron radiation can provide valuable information about the effect of deposition parameters on reaction pathways and reaction kinetics. Such *in situ* studies help researchers achieve a fundamental understanding, on an atomistic level, of the dynamics of thin film formation and phase transformations during thin film synthesis. Wide angle x-ray scattering (WAXS) and small angle x-ray scattering (SAXS) signals simultaneously provide information about phase evolution, defect/stress relaxation, surface structures, and formation of nanostructures. High-intensity, high-energy synchrotron radiation allows for large quantities of diffraction information to be acquired in short time periods (e.g., <1 s) and the small scattering angles associated with high-energy x-rays permit large areas of reciprocal space to be captured with a two-dimensional (2D) detector. High-energy x-rays also exhibit large penetration depths, a necessary attribute for conducting x-ray scattering studies of macroscopic specimens in transmission mode geometry. Figure 1 shows a schematic of the standard transmission mode geometry for synchrotron-radiation based x-ray diffraction studies utilizing a 2D detector.

A range of scientific instruments for *in situ* thin film deposition studies using synchrotron radiation have been reported in the literature, each of the instruments being designed for a specific purpose and each featuring advantageous features.[1–25] We add to this list of synchrotron-radiation based scientific instrumentation for *in situ* thin film deposition studies with a custom-designed ultra-high vacuum (UHV) deposition system (manufactured by PVD Products, Inc.) for industry-relevant thin film growth via magnetron sputtering and cathodic arc deposition. Our deposition system allows *in situ* studies of the synthesis, transformation, and decomposition of thin films via diffraction of high-energy synchrotron radiation. The system has been designed for use at the P07 High Energy Materials Science (HEMS) beamline at PETRA III (Deutsches Elektronen-Synchrotron (DESY); Hamburg, Germany), where the combination of a high photon flux (>10^{12} ph/s) and fast readout 2D detectors (15 Hz) enables the study of highly dynamic processes. The setup uses transmission mode geometry and a wide range of reciprocal space can be investigated with rapid acquisition times (typically 1-30 s with present detectors), which is a stark contrast to the long acquisition times required for many *in situ* deposition systems that are mounted on goniometers and use lower energies.

This *in situ* deposition system was funded by a grant from the Röntgen Ångström Cluster, a collaboration between the governments of Sweden and Germany that promotes collaborative materials research utilizing synchrotron and neutron radiation. The deposition system is versatile and has the potential for a wide range of thin film deposition studies, but our current grant, "*Materials Science of High Performance Cutting*

a)Electronic mail: jersc@ifm.liu.se

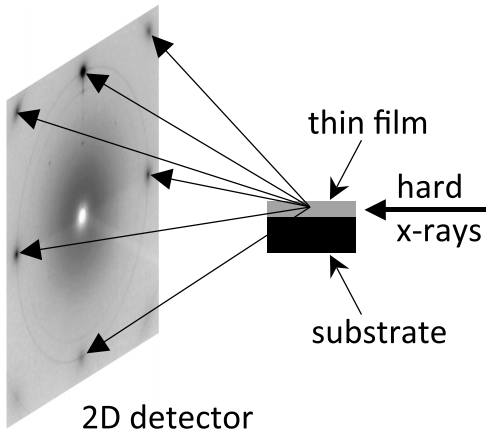

FIG. 1. Schematic of standard transmission-mode geometry for synchrotron-radiation based x-ray diffraction studies utilizing a 2D detector.

Tools Coatings by use of in situ High Energy X-ray Scattering," is focused on the development of enhanced performance hard coatings for cutting tools. The deposition system is dual purpose, incorporating both cathodic arc and magnetron sputtering capabilities. Cathodic arc deposition accounts for the majority of industrial cutting tool PVD coatings while magnetron sputtering is an important method for the fundamental research of thin films as well as being an important industrial process for cutting tool coatings. Our large-scale, *in situ* deposition system enables us to investigate the differences between laboratory-scale and industrial-scale thin film growth, with the aim of easing the transition from academically developed coatings to high-production, industry-relevant coatings. We will be able to investigate the time-evolution of the microstructure during growth and the results will provide further understanding of the interplay between process conditions, nucleation and growth, and nanostructural evolution of future high-performance cutting tool coatings as well as state-of-the-art industrial coatings such as TiAlN.

The reader should keep in mind that synchrotron-based experiments of cutting tool coatings set specific requirements on the design of the sample environment. The sample size is constrained to a size of 5×50 mm^2 to 10×10 mm^2 due to limitations imposed by high-energy synchrotron radiation scattering. Larger sample sizes lead to degraded resolution while smaller sample sizes lead to a reduced diffraction signal. The time resolution of the experimental setup was motivated by realistic deposition rates (>1 Å/s). Fast acting 2D detectors can acquire the necessary diffraction information in short enough time intervals to permit one frame per nanometer of growth. The maximum substrate temperature was motivated by the actual temperatures these coatings experience during cutting operations, which can reach up to 1400 °C. The UHV requirement was imposed in order to conduct experiments with insignificant contamination. Comparative experiments can also be conducted under industrial conditions by intentional degradation of the vacuum (e.g., by synthetic air). The system had to be fully automated for computer interfacing with the beamline and sample alignment requirements necessitated the use of the ultra-high load hexapod at the P07 beamline.

II. OVERVIEW OF DEPOSITION SYSTEM FEATURES

A brief overview of the deposition system is first presented, followed by several sections detailing the more unique features of the system. Figure 2 shows an overview of the deposition system, when configured for magnetron sputtering, in the experimental hutch of the P07 HEMS beamline at PETRA III.

- Four 75 mm diameter DC UHV magnetron sputter sources,
- three 63 mm diameter UHV cathodic arc sources,
- base pressure $<1{\cdot}10^{-7}$ Pa ($<1{\cdot}10^{-9}$ Torr),
- loadlock for rapid sample exchange,
- automated computer control via LabVIEW-based software package,

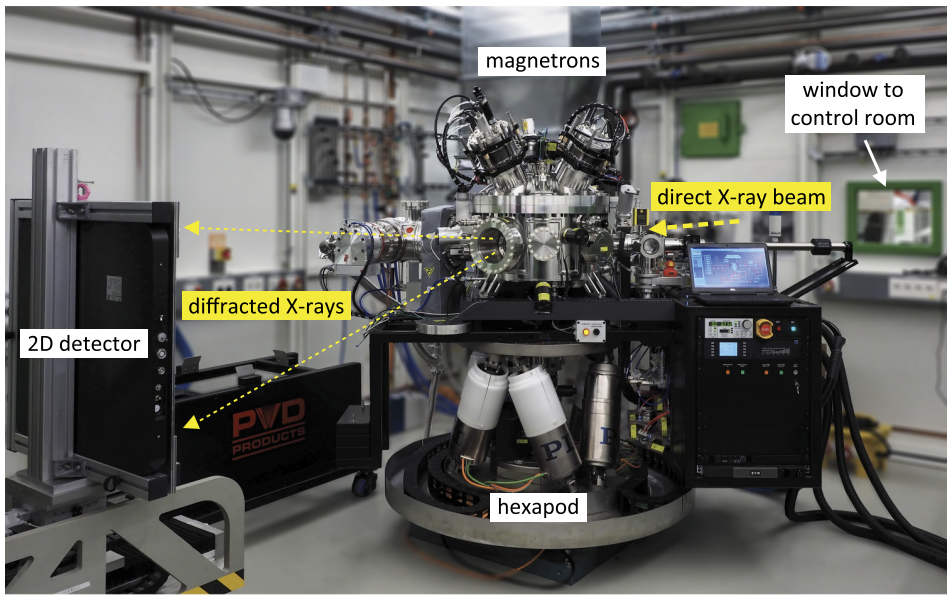

FIG. 2. Configuration of UHV deposition system in the experimental hutch of the P07 HEMS beamline at PETRA III. The deposition system rests on an ultra-high load (1000 kg) hexapod with high resolution 6-axis positioning (x, y, z < 0.8 μm and u, v, w < 0.5 arcsec). A fast-rate 2D detector records x-ray diffraction information. (Note: the background has been blurred to highlight the main features.)

- designed for use on 1-tonne ultra-high load hexapod for high-resolution sample alignment,
- DC (100 V) and RF (125 W) substrate bias,
- laser-based susceptor heating >1400 °C with proportional-integral-derivative (PID) control via spectral band pyrometer,
- film/substrate temperature monitored via 2-colour pyrometer,
- chamber bake-out via internal heat lamps, heat blanket on control gate valve, and heat tape on the vacuum tee of the turbopumps,
- water-cooled chamber walls via serpentine channels welded on outside chamber walls,
- large diameter (600 mm) cylindrical chamber to avoid interaction between sputtering sources and chamber walls,
- uninterruptible power supply (UPS) maintains UHV conditions during temporary electrical failure (<5 min). Experiments immediately resumed upon return of electrical power,
- Inficon quartz crystal monitor on motorized linear stage enables deposition rate calibration at nominal substrate position. Quartz crystal monitor withdrawn during deposition,
- residual gas analyzer (XT100M; ExTorr) for both leak checking and monitoring gas composition during deposition processes,
- ports on chamber lid for kSA Multi-beam Optical Sensor (MOS) to perform real-time *in situ* monitoring of thin film stress, and
- ports for future RHEED system.

III. SPECIFIC FEATURES

A. Magnetron sputtering and cathodic arc evaporation

The UHV deposition system accommodates both magnetron sputtering and cathodic arc deposition via two separate chamber lids. Each chamber lid incorporates a DN600 COF flange using a crimp-on-flange (COF) copper wire seal since standard conflat (CF) flanges are not available in such large diameters. Unlike standard CF flanges that seal via a knife-edge cutting into a copper gasket, COF flanges utilize compression of a copper wire seal with circular cross section. It should be noted that standard industrial magnetron sputtering and cathodic arc systems are high vacuum, not UHV. However, we aim to understand the underlying physics behind the growth of thin films by depositing films in the purest possible environment, hence the UHV requirement. If needed, the UHV deposition system can be made artificially "dirty" through the controlled addition of synthetic air in order to mimic industrial high vacuum conditions.

1. Magnetron chamber lid features (Figures 3(a) and 3(b))

— Four 75 mm diameter DC magnetron sputter sources concentrically oriented with an angle of 35° with respect to the substrate normal (UHV Titan; PVD Products, Inc.),

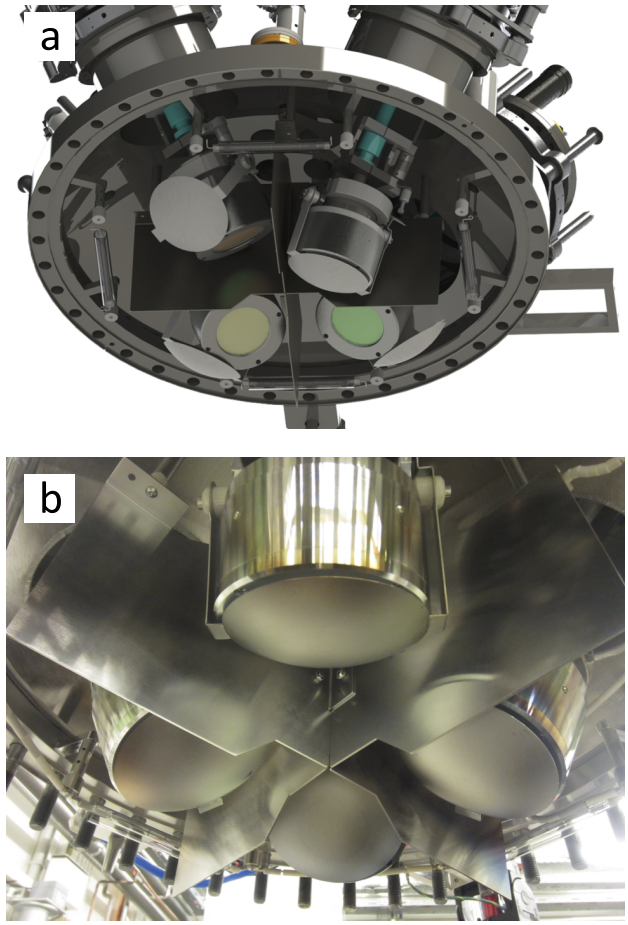

FIG. 3. (a) Schematic of inside view of magnetrons with titanium shutters and mu-metal baffles. The magnetrons are shown at varying z-values and tilt angles. (b) Image of inside view of magnetrons with titanium shutters (all closed) and mu-metal baffles.

— fast-acting, electrically floating, lightweight titanium shutters on each magnetron source,
— manual *in situ* tilting from 18° to 45°, where the angle is defined between the substrate normal and the target normal,
— manual *in situ* target-to-substrate distance adjustment from 130 to 230 mm,
— viewport with two-colour pyrometer for monitoring film/substrate temperature (CellaTemp PA 40; Keller HCW GmbH),
— viewport with universal serial bus (USB) camera for remote substrate viewing,
— two viewports for multi-beam optical sensor (k-Space Associates, Inc.) for *in situ* film stress analysis, and
— high magnetic permeability mu-metal baffles, which are electrically isolated from ground via ceramic standoffs, are situated between adjacent magnetron sources in order to prevent magnetic field interactions as well as minimize cross contamination between magnetrons.

2. Cathodic arc chamber lid features (Figures 4(a)-4(e))

— Three custom-designed 63 mm diameter UHV cathodic arc sources (built in-house at Linköping University; main body manufactured by Thermionics Vacuum Products),

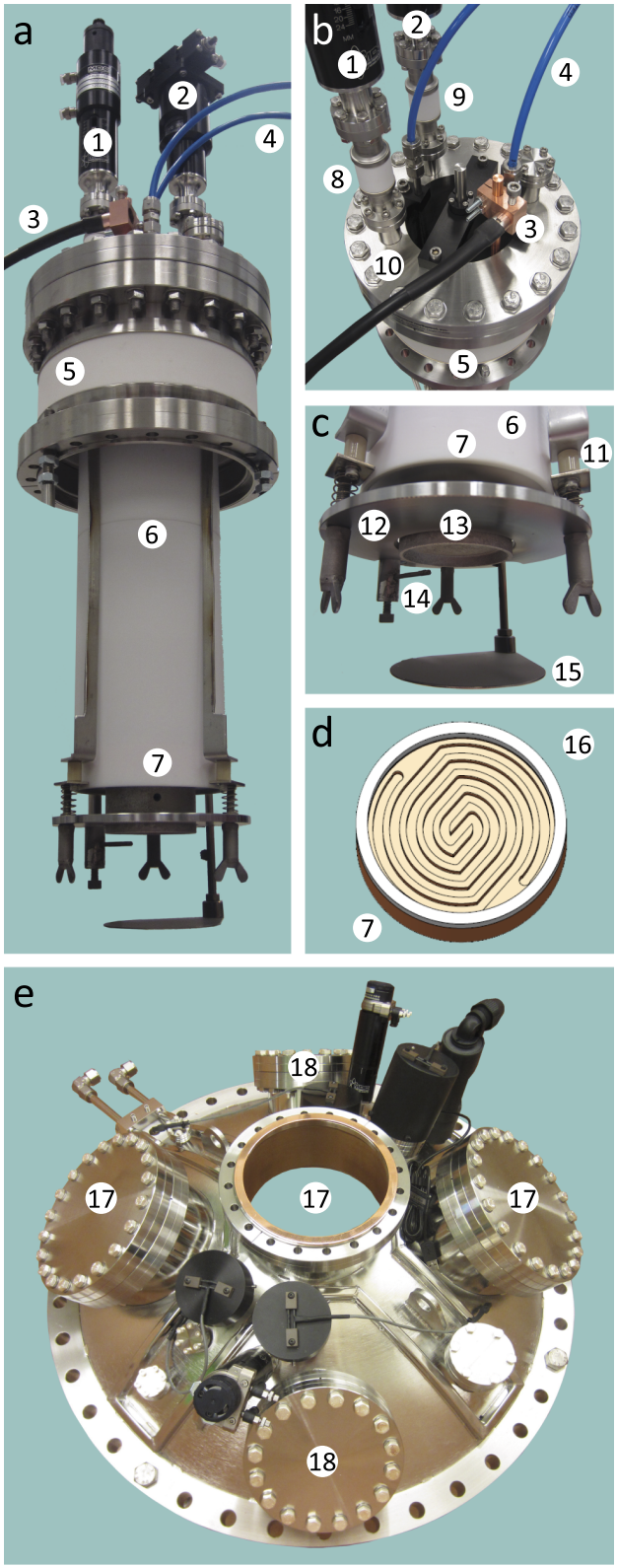

FIG. 4. UHV cathodic arc source (a) overview, (b) external top view, (c) internal target view, (d) water cooled target mounting piece, and (e) chamber lid. Legend for Figure 4. 1. Trigger pin feedthrough, 2. shutter rotary feedthrough, 3. electrical connection, 4. water cooling lines, 5. UHV vacuum ceramic break, 6. Teflon-covered stainless steel tube, 7. explosive-bonded copper-stainless steel, 8. UHV vacuum ceramic break, 9. UHV vacuum ceramic break, 10. adjustable magnet mounting rod, 11. ceramic insulator for carbon steel plate, 12. carbon steel plate, 13. 63 mm O.D. target, 14. tungsten trigger pin, 15. target shutter, 16. water cooling channels, 17. CF flanges for three cathodic arc sources, and 18. spare CF flanges for magnetrons.

— tungsten trigger pin operated via pneumatic linear feedthrough,
— source shutter operated via pneumatic rotary feedthrough,
— two spare DN100CF ports for the future addition of two magnetron sources,
— viewport with two-colour pyrometer for monitoring film/substrate temperature (CellaTemp PA 40; Keller HCW GmbH),
— viewport with USB camera for remote substrate viewing, and
— two viewports for multi-beam optical sensor (k-Space Associates, Inc.) for *in situ* film stress analysis.

The UHV cathodic arc source deserves further attention since industrial cathodic arc sources are designed for HV conditions, not UHV. UHV sources are not commercially available, although a couple other groups have presented designs for UHV cathodic arc sources.[26–29] Our design is highlighted in Figs. 4(a)-4(e). The main body of the cathodic arc source consists of a hollow stainless steel tube welded to a DN160CF flange. The main body is mounted on a CF vacuum ceramic break to electrically isolate the main arc assembly from the main deposition chamber. An explosive-bonded copper-stainless steel piece with water cooling channels is welded to the bottom of the hollow tube. The copper and water cooling channels provide efficient cooling of the target, which is mounted to the copper side of the copper-stainless steel piece. The hollow tube is surrounded by a Teflon tube to prevent the arc from migrating off the target and onto the tube. The arc can be manipulated by a magnet located inside the hollow tube and the position of the magnet relative to the target surface is adjusted with the magnet mounting rod located in the center of the hollow tube. The target is surrounded by a carbon steel plate at floating potential that helps confine the arc to the target surface. The carbon steel plate is electrically isolated from the main arc assembly via three ceramic standoffs and is maintained parallel to the target surface via three manual adjustment nuts. A tungsten trigger pin, which is used to initiate the arc, is controlled via a pneumatic linear feedthrough that is electrically isolated from the main arc assembly via a CF vacuum ceramic break. A target shutter is operated via a pneumatic rotary feedthrough that is also electrically isolated from the main arc assembly via a CF vacuum ceramic break.

B. Hexapod and P07 High Energy Materials Science beamline

The P07 High Energy Materials Science beamline at PETRA III includes a PI (Physik Instrumente) ultra-high load hexapod (prototype M-850K148) capable of supporting equipment up to 1 tonne (1000 kg) (Figure 2). The deposition system was specifically designed for use on this hexapod, an integral component of the experimental setup. The hexapod, a 6-axis positioning system, exhibits high-resolution motor control (x, y, z < 0.8 μm and u, v, w < 0.5 arcsec) with excellent repeatability (x, y, z ± 1 μm and u, v, w < ±1 arcsec), specifications that are critical for fine alignment of the sample with respect to the x-ray beam.

The x-ray energy at P07 is tunable from 30 keV to 200 keV with its main optics consisting of a water-cooled double crystal monochromator in horizontal Laue scattering geometry. The energy resolution ($\Delta E/E$) ranges from 1×10^{-3} down to 7×10^{-5} by changing the curvature of the bent Si(111) crystals in Rowland geometry and/or inserting a channel-cut crystal. The spot size can be varied from 1 mm × 1 mm (unfocused beam) down to 2 μm vertical × 30 μm horizontal (focused beam via Al Compound Refractive Lenses) in high-beta mode or up to 0.9 mm vertical × 6 mm horizontal in low-beta mode, where the beta mode is switched by changing the beta function at the undulator source position. The maximum flux currently reaches 7×10^{11} ph/s at 100 keV.[30,31]

C. Portability: Transferring deposition system to beamline

The deposition system has been designed for portability since it must be moved between a standard laboratory and the experimental hutch of the beamline. The short duration of a single synchrotron beamtime (typically on the order of one week) requires quick and efficient installation of the deposition system on the beamline. It is critical that the system has been fully baked-out and has achieved a low base pressure prior to the start of the beamtime. Bakeout can take a few days while the beamline setup time can be as short as one day. Therefore, the system is baked-out in a standard laboratory prior to the beamtime and the vacuum chamber is isolated and under vacuum during transfer to the beamline.

The deposition system rests on a steel frame when it is housed in the standard laboratory and four heavy duty caster wheels incorporated into the frame allow the system to be easily rolled into the experimental hutch of the beamline. The deposition system is transferred from the steel frame to the hexapod via a 2-tonne overhead crane using lifting straps attached to three lifting bolts integrated on the deposition system frame. Figure 5(a) shows the transfer process and Figure 5(b) shows the deposition system resting on the hexapod. A separate power rack is connected to the deposition system via three main quick-connect cables (Figure 5(c)). Easy transfer and easy hook-up of utilities reduce the time when the deposition system is not under power. The total transfer time can be <1 h and UHV conditions are rapidly restored after system transfer, even if the system has been without power for >12 h.

Many system components and utilities have been incorporated into the main system support structure in order to facilitate the quick and easy transfer of the deposition system, while under vacuum, between the laboratory and the hexapod in the beamline experimental hutch. Incorporating system components and utilities on the main system support structure has the added benefit of lowering the system's center of gravity (required for hexapod specifications) and counterweights have been added to shift the center of gravity to be as close to the sample position as possible.

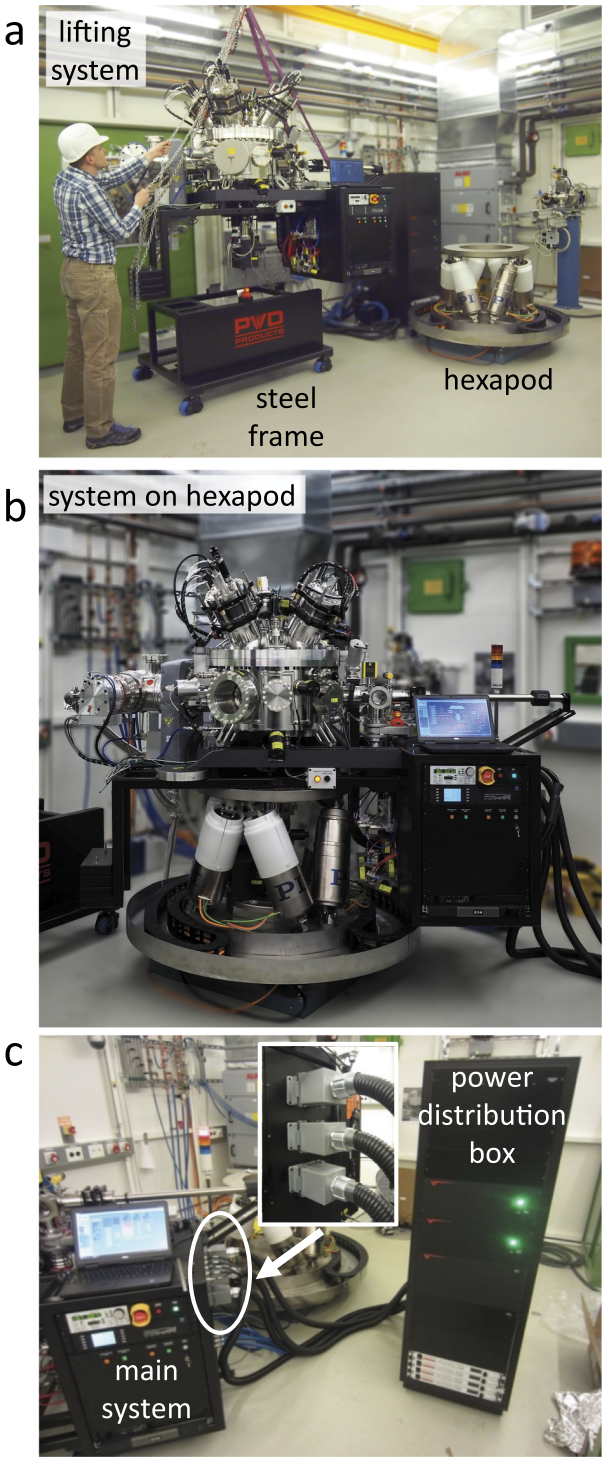

FIG. 5. (a) Transferring the deposition system from the steel frame to the hexapod; (b) deposition system resting on the hexapod at the P07 HEMS beamline of PETRA III; and (c) power distribution box connected to the main system via three quick-connect cables (inset), allowing quick and easy electrical hookup.

D. Computer control

The deposition system is a fully automated computer-controlled system, which allows ease of use and permits automated layer routines for fabricating both simple single layer films and complex multilayer films. All relevant deposition parameters can be controlled via automated layer routines. Automation is achieved with LabVIEW-based software (Figure 6) and an Opto-22 PAC (Programmable Automation Controller). The deposition system software and synchrotron beamline software communicate via a series of potential free contacts

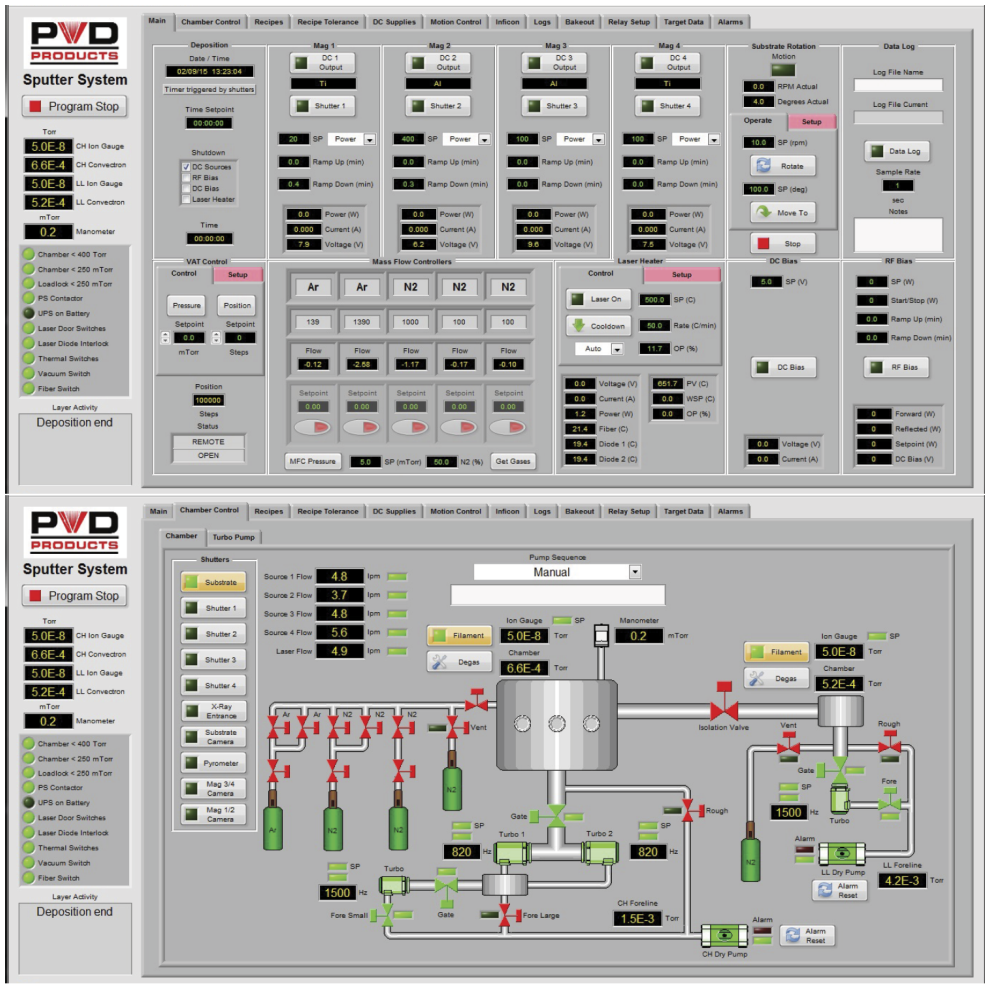

FIG. 6. Representative screenshots of the LabVIEW-based software. The deposition system is fully automated.

(aka dry contacts), allowing for synchronized growth—sample rotation—data acquisition. All critical deposition parameters (e.g., voltage, power, current, gas flows, pressure, and temperature) are logged during growth for post-deposition analysis. A bank of 12 optocoupled relays can be activated in order to protect auxiliary equipment from electric shock in case of uncontrolled arcing in the chamber.

E. Single crystal sapphire viewports as x-ray windows

Many synchrotron-radiation based *in situ* deposition systems utilize beryllium as x-ray transparent windows. We opted for optically transparent single crystal sapphire viewports that provide visual access to the sample, the ability to use alignment lasers, and reduce window heating. Transparent amorphous fused silica viewports were also evaluated, but diffuse x-ray scattering made it difficult to discern diffraction from the film. Figures 7(b)-7(f) show diffraction patterns from a 2 mm thick single crystal sapphire viewport (VG Scienta), a 6.4 mm thick fused silica viewport (Kurt J. Lesker, Co.), a thin film (500 nm ZrN film on silicon substrate), and two film/viewport combinations. All diffraction patterns were acquired with an 87.1 keV x-ray beam. The thin film is still clearly visible when using the single crystal sapphire viewport.

The single crystal sapphire viewports (VG Scienta) are cut with their c-axis normal to the surface. The sapphire viewports can withstand temperatures up to 450 °C, but they will not experience high temperatures given the localized heating of the small substrates, the large distance between the heated substrate and sapphire windows, and the low exposure to thermal radiation that results from the substrate surface being perpendicular to the window surface. The largest commercially available single crystal sapphire viewport has a conflat flange size of DN100CF (6 in. CF) with an 89 mm viewing diameter. The largest diffraction angle of interest is about $\theta = 11°$, corresponding to a minimum d-spacing of 0.4 Å with 80 keV x-rays, which means that the 89 mm diameter sapphire window must be less than 225 mm from the sample to accommodate all diffracted x-rays up to $\theta = 11°$. Because of the large radius of the cylindrical vacuum chamber (300 mm), a re-entrant flange (Figures 7(a) and 8(c)) was incorporated to position the sapphire window 200 mm from the sample.

F. Substrate holder design

Figures 8(a) and 8(b) shows a substrate holder for a 10×10 mm^2 substrate. Substrate holders are fabricated from molybdenum in order to withstand the high substrate temperatures. However, we discovered that the localized heating of the

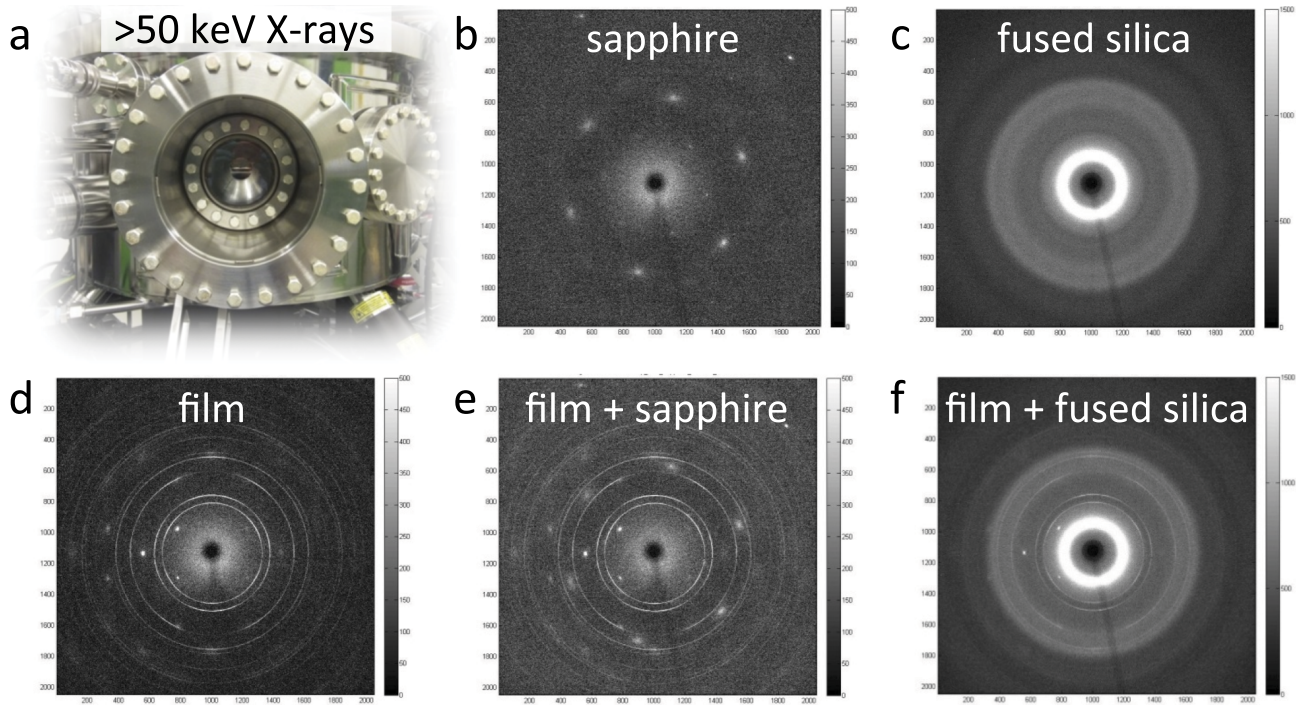

FIG. 7. (a) Diffracted x-rays exit the chamber via a single crystal sapphire viewport mounted on a re-entrant flange; (b) diffractogram of sapphire viewport; (c) diffractogram of fused silica viewport; (d) diffractogram of thin film; (e) diffractogram of thin film and sapphire viewport; and (f) diffractogram of thin film and fused silica viewport.

laser-based heating system results in negligible heating of the substrate holder. The substrate holders incorporate a slanted design to avoid absorption of the downward-directed diffracted x-rays by the holder. The substrate holder can be used with or without optional substrate clips, which are designed to hold the substrate in a fixed position so that it does not move during sample loading. The clips also provide a contact point for applying a substrate bias to the substrate surface. The film/substrate has a 360° field of view without the substrate clips and a more limited field of view when the substrate clips are installed. The substrate holder holds both the laser heater susceptor (see Sec. III I) and the substrate. Figure 8(c) shows an overview of the inside of the chamber. A funnel is attached to the re-entrant flange to prevent film deposition on the sapphire x-ray windows.

G. Pumping system

The main chamber pumping system is equipped with two Pfeiffer Maglev 700 turbopumps placed in parallel on an oversized 200 mm diameter tee to minimize conductance losses (Figure 9). The dual turbo setup allows for (1) process pressures with an unthrottled gate valve and (2) redundancy in case of pump failure.

Depositions can be conducted with or without the throttle valve (e.g., control gate valve). The standard method of controlling process pressure is a throttle valve and a fixed gas flow rate, but this method can result in increased background contamination attributable to the reduced pumping efficiency when the control gate valve is partially closed. On the other hand, maintaining an unthrottled gate valve during deposition and controlling the process pressure via the gas flow rate ensures the lowest possible partial pressure of background contaminants. A gas flow rate of 1000 sccm is required to achieve a process pressure of 2.7 Pa (20 mTorr) with an unthrottled gate valve. High gas throughput turbopumps have argon and nitrogen compression ratios ($>1{\cdot}10^{8}$) that are three orders of magnitude lower than low gas throughput turbopumps ($>1{\cdot}10^{11}$). Our dual turbopump system gives us both a high compression ratio ($>1{\cdot}10^{11}$) and the required high gas throughput (~1000 sccm). Each Pfeiffer Maglev 700 turbopump can accommodate a gas throughput of 474 sccm argon or 770 sccm nitrogen, which results in a maximum gas throughput of 948 sccm argon or 1540 sccm nitrogen for the dual turbopump system.

In addition to providing the necessary compression ratio, pumping speed, and gas throughput, the dual turbopump system has the benefit of redundancy. It is critical that the deposition system does not experience downtime during synchrotron beamtime because of the short and limited beamtime associated with heavily overbooked storage rings. A research group may only get one week of beamtime annually so the likelihood of equipment failure must be minimized. The dual turbopump system is a vital insurance policy against a potential turbopump failure since the deposition system can still function, although to a slightly lesser degree, with a single turbopump.

H. Gas manifold

Process gases enter the main vacuum chamber via the chamber side wall and the gas flow is controlled via high flow rate (1000 sccm) and low flow rate (100 sccm) mass flow controllers (MFCs), one set of high/low flow rate MFCs each

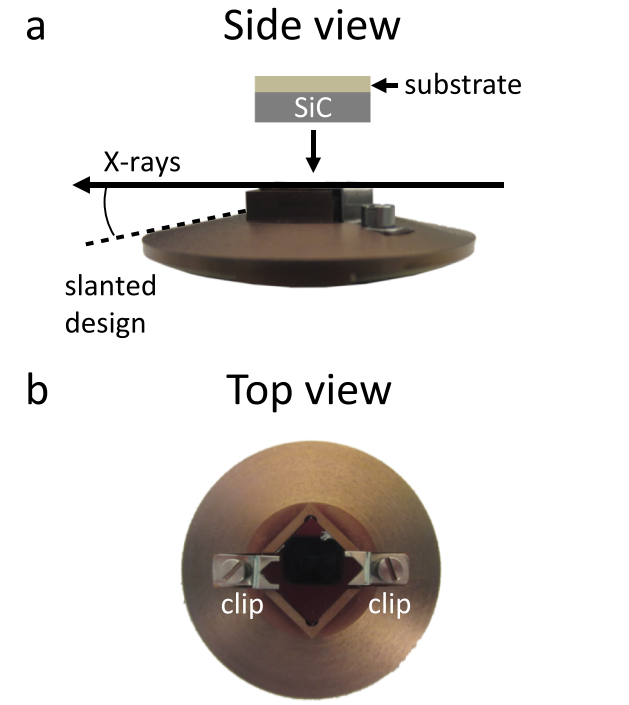

FIG. 8. (a) Side view and (b) top view of molybdenum sample holder for 10×10 mm substrates. The slanted design prevents absorption of diffracted x-ray intensity; (c) inside view of vacuum chamber. Funnel between substrate and re-entrant flange protects the sapphire viewport from deposition.

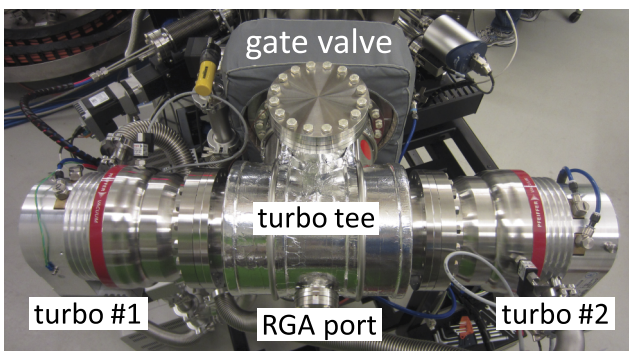

FIG. 9. Dual parallel turbopump system provides a high compression ratio and a high gas throughput.

for both argon and nitrogen. The high flow rate MFCs are employed when depositing with an unthrottled gate valve since high flow rates (56-995 sccm) are required to achieve deposition pressures in the range of 0.3-2.7 Pa (2-20 mTorr). Because of the high pumping speed, the process pressure is not highly sensitive to changes in the gas flow rate when operating with an unthrottled gate valve. For example, a flow rate change of 10 sccm results in a 0.01 Pa (0.1 mTorr) change in pressure. The low flow rate MFCs are employed when controlling the process pressure via the control gate valve since lower gas flows are required.

Process gases consist of 99.999% argon and 99.999% nitrogen that are further purified by gas purifiers (Entegris Gatekeeper; <1 ppb for H_2, CO, CO_2; <100 ppb for H_2 O, O_2) located before each set of high/low flow rate MFCs, ensuring a supply of ultra-high purity process gas (>99.999 998%).

I. Laser heater

Substrate heating is achieved via a laser-based system consisting of an 808 nm infrared laser diode (Dilas Diode Laser, Inc.) powered by a 300 W power supply (Lumina Power, Inc.) (Figure 10). The laser beam heats a susceptor material, in this case silicon carbide (SiC), which then heats the substrate via thermal conduction and radiation. The laser beam is directed along a fiber optic cable to a beam expander (Laser Motive) for adjusting the beam diameter to the size of the susceptor. The adjusted laser beam is then reflected off a mirror before entering the chamber through an 808 nm AR-coated quartz viewport (ZrO_2/SiO_2-based coating). The laser beam, with circular cross section, strikes the backside of a 10 × 10 mm SiC susceptor with a thickness of 1.6 mm. SiC was selected as the susceptor material because of its high absorption of 808 nm radiation (emissivity value 0.96-0.99), high thermal conductivity (~150 W/m-K), and excellent thermal shock resistance. The SiC temperature is controlled via a spectral band pyrometer (LumaSense Technologies, Inc.) that is focused on the backside of the SiC susceptor. The deposition substrate is placed in direct contact with the polished front side of the SiC susceptor. No thermal pastes or intermediate thermal interface materials are used between the deposition substrate and the SiC susceptor, which otherwise might degrade the UHV environment. A separate two-colour pyrometer (CellaTemp PA 40 (KELLER HCW GmbH) with close-up lens; 650-1700 °C temperature range; spot size of 5.3 mm at a focal length of 400 mm) is incorporated on the chamber lid to directly monitor the film/substrate temperature from the front side.

The laser-based heating system offers many advantages over conventional indirect resistive-based heating systems. Laser-based heaters offer "clean" heating in both UHV environments and in a variety of background gas environments over a wide pressure range. Standard resistive-based heaters can liberate a variety of gasses (e.g., CO, CO_2, H_2O, and H_2) depending on the heater design while laser-based heating systems exhibit reduced outgassing due to localized heating of the susceptor and reduced heating of vacuum components by sample radiation, a consequence of the lower power requirements for localized heating. Although we employ a SiC

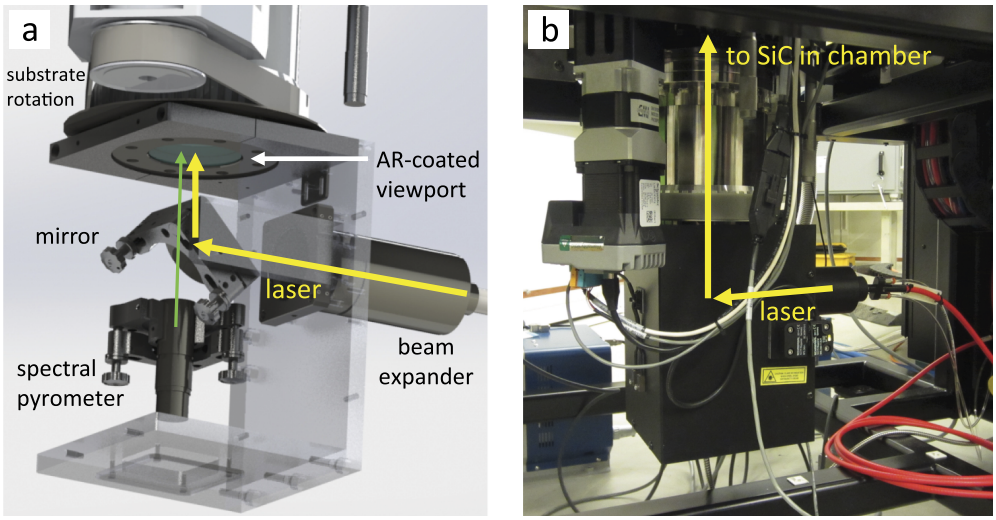

FIG. 10. (a) Schematic of internal construction of the laser-based heater assembly located on the bottom of the vacuum chamber. The 808 nm laser beam (yellow arrow) travels through a fiber optic cable, passes through a beam expander, reflects off a mirror, enters the vacuum chamber via an AR-coated quartz viewport, and strikes the backside of a SiC susceptor. The susceptor temperature is controlled via a spectral pyrometer (green arrow) pointing at the same location on the SiC susceptor as the laser. (b) Image of a section of the laser-based heater assembly located on the bottom of the vacuum chamber.

susceptor, direct heating of non-transparent substrates (e.g., silicon) is also possible, further reducing outgassing. Internal components such as power leads, thermocouples, and water cooling lines are not required in laser-based heating systems and substrate rotation is easy to implement.

Maximum temperature is another distinct advantage of our laser-based heating system, providing the possibility to perform deposition and annealing studies at temperatures much higher (>1400 °C) than what is possible with conventional resistive-based heating systems (~900 °C). The maximum temperature of a conventional heater is typically limited by the temperature constraints of the electrical connections whereas the laser-based heating system is limited by the susceptor material. In addition to a higher maximum temperature, fast heating and cooling rates can be achieved because of the localized heating of the susceptor (or non-transparent substrate) and the laser spot size can be adjusted to accommodate varying sample sizes.

The main drawback of the laser-based heating system is laser safety concerns related to the Class 4 IR diode laser. The chamber viewports must be blocked during laser operation in order to ensure that the deposition system as a whole is classified as a Class 1 laser system (standard IEC 60825-1). It is therefore not possible to use the naked eye to look into the vacuum chamber during deposition at elevated temperatures. We circumvent this issue with multiple USB web cameras directed at the substrate and deposition sources. The cameras were also motivated by hard X-ray safety guidelines, which require that the system be remotely operated from a separate control room when conducting synchrotron radiation experiments. In addition to protecting the user, we have also implemented safety features to protect the deposition system from potential damage caused by the laser. Thermal sensors have been mounted in key locations in the unlikely event that the laser escapes the confines of the laser-heating system. The top of the chamber lid is the most likely location for the laser to strike in the event of a SiC susceptor failure, so thermal sensors are located on the exterior top of the chamber lid. The software is also programmed to automatically shut off the laser when the spectral band pyrometer reading varies substantially from the setpoint temperature, a possible indicator of a missing or failed SiC susceptor.

J. Substrate rotation

Substrate rotation is achieved via a stepper motor with a 3600 step encoder. A 1:10 gearing ratio between the stepper motor and substrate enables 36 000 steps per revolution, resulting in a nominal resolution of 0.009°. The fine resolution is necessary to accurately and repeatedly acquire diffraction images at specific azimuthal angles each time, which is of particular importance when studying epitaxial growth. Depending on the crystal quality, images are acquired either during substrate rotation or with a stationary sample. The diffraction image from random polycrystalline thin films (i.e., diffraction rings) is independent of sample orientation, thus allowing for continuous sample rotation during image acquisition. However, the diffraction image from epitaxial films (i.e., diffraction spots) is sample-orientation dependent, thereby requiring a stationary sample during image acquisition. For epitaxial and orientation-dependent films, the deposition system software and stepper motor enable the user to stop precisely and repeatedly at specific user-defined crystallographic directions in order to acquire diffractograms. Communication between the deposition system and image acquisition software occurs via a series of potential free contacts (aka dry contacts). Film deposition can continue or be paused during image acquisition. After image acquisition, the beamline software sends a signal to the deposition system in order to resume the deposition process and substrate rotation. The number of substrate revolutions between each image acquisition is predefined by the user in the software's layer routine, which is a recipe describing the complete deposition process.

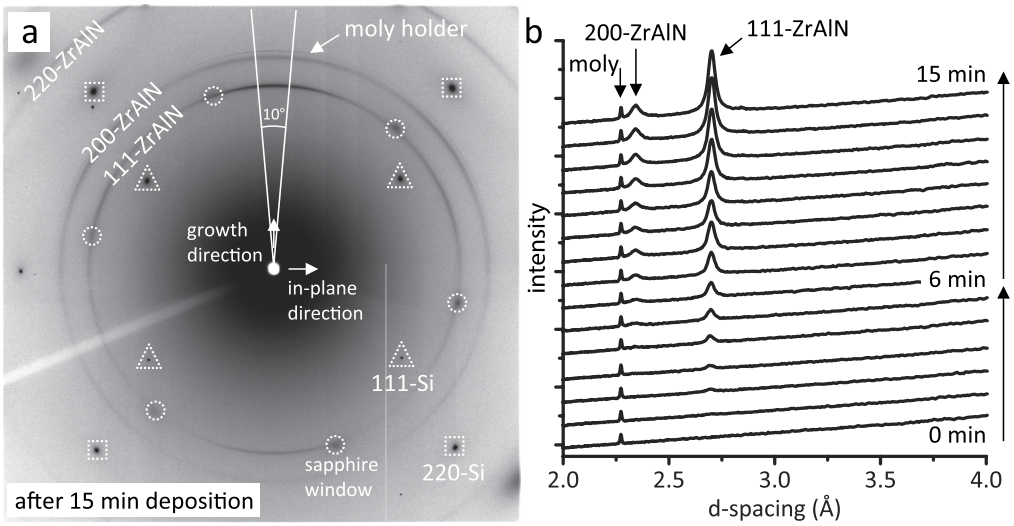

FIG. 11. (a) 2D synchrotron-based x-ray diffraction pattern of a $Zr_{0.75}Al_{0.25}N$ thin film imaged during deposition on a 100-silicon substrate. The image was acquired during a full 360° revolution at 15 min into the deposition (~300 nm thick). (b) The deposition process can be characterized by analyzing lineouts versus deposition time. The lineouts shown are the mean intensity of the 10° region highlighted in (a). The lineouts have been offset for clarity.

IV. TRIAL DEMONSTRATION OF *IN SITU* X-RAY DIFFRACTION DURING THIN FILM GROWTH

Detailed experimental results from a range of materials systems are forthcoming from upcoming beamtimes and will be published elsewhere. However, we were able to conduct a trial test to demonstrate the capability of our deposition system to acquire time-resolved x-ray diffraction data during thin film growth. We deposited a 300 nm $Zr_{0.75}Al_{0.25}N$ thin film on a 100-silicon substrate at 700 °C via reactive dc-magnetron sputtering in a 5 mTorr 10%N_2/90%Ar ambient from a $Zr_{0.75}Al_{0.25}$ target (76 mm diameter × 6 mm thick). The film was deposited for 15 min at 400 W, yielding a deposition rate of 20 nm/min. The target to substrate distance was 15 cm and the substrate rotation speed was 7.5 rpm. The base pressure was $2.7 \cdot 10^{-7}$ Pa ($2.0 \cdot 10^{-9}$ Torr).

Eight second exposures were acquired every 30 s using a 200 μm high × 700 μm wide x-ray beam at 78 keV. Each image was acquired over a full 360° revolution, so the images include diffraction information from a 3D volume of reciprocal space. This imaging procedure is in contrast to imaging at a fixed substrate position, whereby the image is a 2D slice of reciprocal space. Imaging during substrate rotation causes the 2D slice of reciprocal space to sweep around the substrate normal, thereby capturing a 3D volume. Additional imaging must be acquired at fixed substrate positions to determine the orientational relationships between the film and substrate.

Diffraction images acquired during thin film growth can be post-processed to characterize the details of the thin film growth process. Figure 11(a) shows a representative 2D diffractogram after depositing for 15 min and Figure 11(b) presents the evolution of the 111-ZrAlN and 200-ZrAlN peaks (in the growth direction) during film growth. We can additionally characterize the growth process in different directions and evaluate the time-resolved behavior of such parameters as d-spacing and full-width-at-half-maximum (FWHM).

V. SUMMARY

We introduced a new state-of-the-art UHV deposition system for time-resolved *in situ* investigation of thin film deposition processes using high-energy synchrotron radiation. The system is capable of both magnetron sputtering and cathodic arc deposition under industry-relevant conditions. The deposition system is a valuable addition to the infrastructure of PETRA III at DESY, being specifically designed for use on the 1-tonne ultra-high load hexapod at the P07 HEMS beamline. A trial test of a time-resolved deposition process was presented while detailed experimental results from a range of materials systems are forthcoming and will be published elsewhere. We strongly welcome and encourage collaboration from the materials science research community in order to maximize the potential of this unique *in situ* deposition system for improving understanding of fundamental thin film deposition processes.

ACKNOWLEDGMENTS

We acknowledge financial support from the Swedish Research Council via the Röntgen Ångström Cluster (RÅC) Frame Program (No. 2011-6505) and the German Federal Ministry of Education and Research (BMBF) under Grant No. 05K12CG1.

[1]S. Brennan, P. H. Fuoss, J. L. Kahn, and D. W. Kisker, "Experimental considerations for *in situ* x-ray scattering analysis of OMVPE growth," Nucl. Instrum. Methods Phys. Res., Sect. A **291**, 86–92 (1990).
[2]J. Q. Zheng, M. C. Shih, X. K. Wang, S. Williams, P. Dutta, R. P. H. Chang, and J. B. Ketterson, "A miniature x-ray compatible sputtering system for studying *in situ* high Tc thin film growth," J. Vac. Sci. Technol., A **9**, 128–132 (1991).
[3]A. P. Payne, B. M. Clemens, and S. Brennan, "An apparatus for studying sputter deposition with x-rays," Rev. Sci. Instrum. **63**, 1147–1149 (1992).
[4]S. Williams, J. Q. Zheng, M. C. Shih, X. K. Wang, S. J. Lee, E. D. Rippert, S. Maglic, H. Kajiyama, D. Segel, P. Dutta, R. P. H. Chang, J. B. Ketterson,

T. Roberts, Y. Lin, R. T. Kampwirth, and K. Gray, "*In situ* x-ray diffraction studies of $YBa_2Cu_3O_x$," J. Appl. Phys. **72**, 4798–4804 (1992).
[5]H. You, R. P. Chiarello, H. K. Kim, and K. G. Vandervoort, "X-ray reflectivity and scanning-tunneling-microscope study of kinetic roughening of sputter-deposited gold films during growth," Phys. Rev. Lett. **70**, 2900–2903 (1993).
[6]S. M. Williams, H. Q. Yang, and J. B. Ketterson, "Miniature multitarget sputtering system for the *in-situ* x-ray study of high T_c multilayer film growth," J. Vac. Sci. Technol., A **12**, 598–600 (1994).
[7]S. Ferrer and F. Comin, "Surface diffraction beamline at ESRF," Rev. Sci. Instrum. **66**, 1674–1676 (1995).
[8]R. L. Headrick, S. Kycia, Y. K. Park, A. R. Woll, and J. D. Brock, "Real-time x-ray-scattering measurement of the nucleation kinetics of cubic gallium nitride on beta-SiC(001)," Phys. Rev. B **54**, 14686–14691 (1996).
[9]H. You, K. G. Huang, and R. T. Kampwirth, "Off-specular reflectivity study of sputter-deposition of platinum during growth," Physica B **221**, 77–85 (1996).
[10]J. H. Je, D. Y. Noh, H. K. Kim, and K. S. Liang, "Preferred orientation of TiN films studied by a real time synchrotron x-ray scattering," J. Appl. Phys. **81**, 6126–6133 (1997).
[11]G. B. Stephenson, J. A. Eastman, O. Auciello, A. Munkholm, C. Thompson, P. H. Fuoss, P. Fini, S. P. DenBaars, and J. S. Speck, "Real-time X-ray scattering studies of surface structure during metalorganic: Chemical vapor deposition of GaN," MRS Bull. **24**, 21–25 (1999).
[12]H. Y. Lee, K. S. Liang, C. H. Lee, and T. B. Wu, "Real-time x-ray scattering study of growth behavior of sputter-deposited $LaNiO_3$ thin films on Si substrates," J. Mater. Res. **15**, 2606–2611 (2000).
[13]W. Matz, N. Schell, W. Neumann, J. Bottiger, and J. Chevallier, "A two magnetron sputter deposition chamber for *in situ* observation of thin film growth by synchrotron radiation scattering," Rev. Sci. Instrum. **72**, 3344–3348 (2001).
[14]K. Ellmer, R. Mientus, V. Weiss, and H. Rossner, "*In situ* energy-dispersive x-ray diffraction system for time-resolved thin-film growth studies," Meas. Sci. Technol. **14**, 336–345 (2003).
[15]D. Lutzenkirchen-Hecht, K. Bruder, U. Haake, P. Keil, C. Markert, C. Ringpfeil, and R. Frahm, "Miniaturized multipurpose cell for *in situ* investigation of sputtered thin films with x-ray techniques," Rev. Sci. Instrum. **76**, 073905 (2005).
[16]P. R. Willmott, C. M. Schleputz, B. D. Patterson, R. Herger, A. Lange, D. Meister, D. Maden, C. Bronnimann, E. F. Eikenberry, G. Hulsen, and A. Al-Adwan, "*In situ* studies of complex PLD-grown films using hard X-ray surface diffraction," Appl. Surf. Sci. **247**, 188–196 (2005).
[17]Y. C. Liang, H. Y. Lee, H. J. Liu, and Y. W. Hsieh, "An off-axis magnetron-sputtering system for *in situ* studies of artificial superlattices growth by synchrotron radiation scattering," J. Synchrotron Radiat. **14**, 163–168 (2007).
[18]N. Schell, J. von Borany, and J. Hauser, "A two magnetron sputter deposition chamber equipped with an additional ion gun for *in situ* observation of thin film growth and surface modification by synchrotron radiation scattering," AIP Conf. Proc. **879**, 1813–1816 (2007).
[19]S. Couet, T. Diederich, K. Schlage, and R. Rohlsberger, "A compact UHV deposition system for *in situ* study of ultrathin films via hard x-ray scattering and spectroscopy," Rev. Sci. Instrum. **79**, 093908 (2008).
[20]Y. J. Park, D. R. Lee, H. H. Lee, H. B. R. Lee, H. Kim, G. C. Park, S. W. Rhee, and S. Baik, "*In-Situ* synchrotron x-ray scattering study of thin film growth by atomic layer deposition," J. Nanosci. Nanotechnol. **11**, 1577–1580 (2011).
[21]B. Krause, S. Darma, M. Kaufholz, H. H. Grafe, S. Ulrich, M. Mantilla, R. Weigel, S. Rembold, and T. Baumbach, "Modular deposition chamber for *in situ* X-ray experiments during RF and DC magnetron sputtering," J. Synchrotron Radiat. **19**, 216–222 (2012).
[22]J. Burgi, R. Neuenschwander, G. Kellermann, J. Garcia Molleja, A. F. Craievich, and J. Feugeas, "Reactive sputter magnetron reactor for preparation of thin films and simultaneous *in situ* structural study by X-ray diffraction," Rev. Sci. Instrum. **84**, 015102 (2013).
[23]R. Dohrmann, S. Botta, A. Buffet, G. Santoro, K. Schlage, M. Schwartzkopf, S. Bommel, J. F. H. Risch, R. Mannweiler, S. Brunner, E. Metwalli, P. Muller-Buschbaum, and S. V. Roth, "A new highly automated sputter equipment for *in situ* investigation of deposition processes with synchrotron radiation," Rev. Sci. Instrum. **84**, 043901 (2013).
[24]S. Bauer, S. Lazarev, A. Molinari, A. Breitenstein, P. Leufke, R. Kruk, H. Hahn, and T. Baumbach, "The power of *in situ* pulsed laser deposition synchrotron characterization for the detection of domain formation during growth of $Ba_{0.5}Sr_{0.5}TiO_3$ on MgO," J. Synchrotron Radiat. **21**, 386–394 (2014).
[25]S. Ibrahimkutty, A. Seiler, T. Prussmann, T. Vitova, R. Pradip, O. Bauder, P. Wochner, A. Plech, T. Baumbach, and S. Stankov, "A portable ultrahigh-vacuum system for advanced synchrotron radiation studies of thin films and nanostructures: $EuSi_2$ nano-islands," J. Synchrotron Radiat. **22**, 91–98 (2015).
[26]D. Isfort and V. Buck, "Development of a UHV compatible hollow cathode arc source for the deposition of hard nitride coatings," Plasma Sources Sci. Technol. **9**, 25–31 (2000).
[27]R. Russo, L. Catani, A. Cianchi, D. DiGiovenale, J. Lorkiewicz, S. Tazzari, C. Granata, P. Ventrella, G. Lamura, and A. Andreone, "Niobium coating of cavities using cathodic arc," IEEE Trans. Appl. Supercond. **19**, 1394–1398 (2009).
[28]R. Russo, L. Catani, A. Cianchi, S. Tazzari, and J. Langner, "High quality superconducting niobium films produced by an ultra-high vacuum cathodic arc," Supercond. Sci. Technol. **18**, L41–L44 (2005).
[29]R. Russo, A. Cianchi, Y. H. Akhmadeev, L. Catani, J. Langner, J. Lorkiewicz, R. Polini, B. Ruggiero, M. J. Sadowski, S. Tazzari, and N. N. Koval, "UHV arc for high quality film deposition," Surf. Coat. Tech. **201**, 3987–3992 (2006).
[30]N. Schell, A. King, F. Beckmann, T. Fischer, M. Müller, and A. Schreyer, "The high energy materials science beamline (HEMS) at PETRA III," Mater. Sci. Forum **772**, 57–61 (2014).
[31]See http://photon-science.desy.de/facilities/petra_iii/beamlines/p07_high_energy_materials_science/index_eng.html for specific and detailed information about P07, the High Energy Materials Science Beamline of Helmholtz-Zentrum Geesthacht (HZG) and DESY.